Long-wave phonons in ZnSe-BeSe mixed crystals: Raman scattering and percolation model

O. Pagès,* M. Ajjoun, and T. Tite
Institut de Physique, Université de Metz, 57078 Metz, France

D. Bormann
Laboratoire de Physico-Chimie des Interfaces et Applications, Université d'Artois, 62037 Lens, France

E. Tournié†
Centre de Recherche sur l'Hétéroépitaxie et ses Applications, Rue Gregory, 06560 Valbonne, France

K. C. Rustagi
Center for Advanced Technology, Indore 452013, India

(Received 18 November 2003; revised manuscript received 24 March 2004; published 21 October 2004)

We extend to longitudinal-optical (LO) phonons the percolation model set for the basic understanding of the atypical transverse-optical (TO) one-bond→two-mode behavior observed by Raman scattering in the Be-Se spectral range of the random $Zn_{1-x}Be_xSe$ alloy ($0 \leqslant x \leqslant 1$), which opens the class of mixed crystals with contrast in the bond stiffness. The study is supported by contour modeling of the TO and LO Raman line shapes. This is achieved via application of the Hon and Faust treatment to a version of the modified-random-element-isodisplacement model generalized to multioscillators. While the TO signal clearly discriminates between Be-Se vibrations within the hard Be-rich region and the soft Zn-rich one, complexity arises in the LO symmetry due to vibration coupling via the 1ong-range longitudinal polarization field. In particular this generates a massive transfer of oscillator strength from the low-frequency (LO^-) (hard, soft)-mixed mode to the high-frequency (LO^+) one, which results in an apparent LO^+ single-mode behavior. Moreover the contrasts between the Zn-Se and Be-Se bond lengths and bond stiffness are proposed to force a Verleur and Barker-like (VB) discrete multimode Raman response from each region. Accordingly LO^- and LO^+ intramode transfers of oscillator strength superimpose to the $LO^- \rightarrow LO^+$ intermode one. This accounts for the spectacular distortions of the LO^+ line shape. On the whole, the puzzling LO behavior can be regarded as the result of a cooperative phenomenon between two discrete assemblies of polar LO phonons, driven by the long-range longitudinal polarization field. Also, the Verleur and Barker description accounts for subtle unexplained behaviors in the TO symmetry. More generally it appears to provide a much attractive area for the discussion of the asymmetries of the TO and LO Raman line shapes in random alloys, as a possible alternative to the much debated spatial correlation model or to internal/external strain effects.

DOI: 10.1103/PhysRevB.70.155319 PACS number(s): 78.30.Fs, 63.20.Pw, 64.60.Ak

I. INTRODUCTION

The vibrational properties in the optical range of the ternary semiconductor $A_{1-x}B_xC$ mixed crystals have been investigated by various techniques over the past 50 years, and are well documented both experimentally and theoretically. Reviews of earlier experimental and theoretical works in this area can be found in Ref. 1. Although the problem is intrinsically a complicated one, most of the experimental data related to long wave ($q \sim 0$) phonons fit in the one-bond →one-mode behavior as envisaged by the modified-random-element-isodisplacement (MREI) model from Chang and Mitra.[2] Under certain conditions this can also be made to work for the alloys that exhibit the much less frequent two-bond→one-mode behavior. The latter so-called mixed-mode behavior reduces thereby to a special case of the MREI model.[2] This can be described as a VCA (virtual crystal approximation) model since the alloy is viewed as perfectly homogeneous at the local scale. For instance the *C* atoms, from the unperturbed site, are all supposed to experience the same mechanical forces produced by a statistical average of A and B nearest neighbors depending on *x*.

Our view is that the vibrational properties in mixed crystals should not accommodate in principle to a VCA description, because these are bond-related and thereby local in nature. Accordingly local insight upon the topology of the substituting species would be needed for their basic understanding. This relates directly to the percolation theory,[3] which remains basically unexplored regarding vibrational properties of mixed crystals. Precisely we have shown in earlier work[4–6] that the arriving mixed crystals with (Be, N) in substitutional positions, which exhibit a large contrast in the bond stiffness, are choice systems for the investigation of percolation behaviors regarding bond vibrations. *Ab initio* calculations performed by Bellaiche, Wei, and Zunger (Ref. 7) have demonstrated that the same holds basically true for percolation-induced bond-length anomalies. This is because the percolation effects upon the physical properties of the *stiff* bond seem to be exacerbated in such contrasted systems.[7]

Nitrogen does not mix well in semiconductors, i.e., only a small fraction can be incorporated in substitutional position.

For instance in $GaAs_{1-x}N_x$, which attracts much attention due to a giant band-gap reduction at small x,[8] phase separation occurs from the critical N content of $\sim 2-3\%$.[9] The same holds true in the more recent $GaP_{1-x}N_x$ alloy, with similar band-gap properties.[10] One presumed reason for the "demixing" of nitrogen in the above alloys is that the spectacular bulk modulus of GaN, about four times larger than the III-V standard, goes with a drastic reduction of $\sim 20\%$ in the bond length, which altogether creates dramatic local bond distortions in the alloy. Accordingly now available N-based systems are excluded for sound experimental investigation of percolation effects upon the bond properties.

The mechanical contrast between the Be- and Zn-based compounds is not concerned with the bond-stretching force constant, as in the N-based systems, but with the bond-bending force constant, which relates to the shear modulus C_s^*. This is due to the large amount of covalent bonding in Be chalcogenides,[11] while the N-based bonds remain highly ionic in character. The calculated C_{ij} values in Be chalcogenides[12] provide C_s^* estimates around 0.478 and 0.510 in BeSe and BeTe, respectively, i.e., roughly twice the values for ZnSe(0.277) and ZnTe(0.319).[13] Accordingly the mechanical contrast is much smaller in the Be-based alloys than in the N-based ones. Moreover the lattice mismatch falls down to $\sim 9\%$. Altogether this might explain why random $Zn_{1-x}Be_x(Se,Te)$ mixed crystals of high quality, regarding x-ray measurements, can be formed over wide composition ranges.[4,5] In particular, the full range is available with ZnBeSe, while the Be content is limited to ~ 0.5 in ZnBeTe. This offers much interesting opportunity for detailed investigation of percolation effects upon the physical properties of the stiff Be-VI bond.

Precisely, we have investigated Raman spectra of the $Zn_{1-x}Be_x(Se,Te)$ alloys in a series of well-characterized (001) epitaxial layers in recent years.[4,5,14,15] Most of the attention was awarded to the long-wave transverse-optical (TO) modes, because these consist of quasi-independent oscillators, and thereby carry clear information. Complexity arises in the longitudinal-optical (LO) symmetry, due to coupling via the macroscopic polarization field.

The same atypical one-bond→two-mode TO behavior could be observed in the vibrational range of the stiff Be-VI bond in ZnBeSe and ZnBeTe. This was explained by using a double-branch percolation picture which discriminates between vibrations within the randomly formed hard Be-rich host region and the soft Zn-rich one. Also, each branch displays both a cluster and a continuum regime, according to the topology of the host region. The "cluster → continuum" transition occurs at the so-called percolation threshold. From numerical simulations based on random substitution on the cfc-(Zn,Be) sublattice, this is estimated at $x_{\text{Be-VI}}=0.19$ for the Be-rich region and at $x_{\text{Zn-VI}}=0.81$ for the Zn-rich one.[3] Besides simple symmetry considerations indicate that the volume of the Be- and Zn-rich regions scale as x and $1-x$, respectively. Accordingly the strengths of the Be-VI modes from the Be- and Zn-rich regions scale ideally as x^2 and $x(1-x)$, respectively. More detail is given below (refer to Sec. III B).

Recently we have derived on the above basis a simplified double-branch percolation picture for the two *softlike* bonds in standard $A_{1-x}B_xC$ mixed crystals, i.e., with no contrast in the bond stiffness. This allowed to achieve simple understanding of the much debatted $q\sim 0$ multiphonon behavior in GaInAs, considered as a typical challenging system.[16] Accordingly the double-branch percolation picture takes a universal character, and there is a need of sound investigation, which comes to the stiff Be-VI bond in the ZnBeVI alloys. While reasonable understanding of the multiphonon Be-VI behavior is achieved in the TO symmetry, the LO behavior remains unexplained.

More precisely, a preliminary quantitative approach was proposed for contour modeling of the Be-Se TO and LO Raman line shapes.[4] As a rather crude approximation these were taken as the simple addition of standard one-bond →one-mode Raman signals from the hard and soft regions, weighted by their relative scattering volume, which supposed the consideration of separate dielectric functions for the two host regions. The model provided a reasonable understanding of the optical-phonon behavior, but limited to the TO modes. Still, subtle antagonism in the asymmetries of the dominant TO lines at the two ends of the percolation range was not discussed. Most of all, the LO symmetry remained highly disconcerting. Neither the systematic overdamping of the low-frequency LO mode nor the marked red asymmetry of the high-frequency one could be explained.

Let us emphasize that the two characters have no equivalent in the TO symmetry. In particular, the strength balance between the two TO modes is highly x sensitive. Also, the high-frequency LO mode is located at much higher frequency than predicted. At last the monotonous decrease of the LO linewidth when x increases throughout the percolation range could not be explained.

In the present work we push further the Raman study of the Be-Se one-bond→two-mode behavior in the LO symmetry. The discussion is supported by extensive Raman data and full contour modeling of the TO and LO Raman line shapes via a one-bond→multimode description. A single dielectric function is used to describe the hard/soft-composite ZnBeSe crystal.

The paper is organized as follows: The experimental details are given in Sec. II. A brief outline of the Hon-and-Faust/MREI model generalized to multioscillators that we derive for contour modeling of the TO and LO Raman line shapes is given in Sec. III. Also, the TO double-branch Be-Se picture is detailed in this section, with strong experimental support, as a basis for the LO discussion. This occupies Sec. IV. Reasonable understanding of the LO line shapes requires further multimode decomposition of the apparently single-mode signals from the hard and soft regions. Continuous decomposition, as qualitatively suggested by Brafman and Manor,[17] as well as discrete decomposition, on the Verleur and Barker basis,[18,19] are successively investigated. In any case the key role of the long-range longitudinal polarization field as a carrier of coherence in LO multiphonon polar systems is highlighted. At last, we investigate whether multimode decomposition may provide any insight upon the disconcerting Be-Se TO and LO asymmetries. Also, we discuss a possible reason why the multimode description is pertinent in the Be-based systems. Conclusions are summarized in Sec. V.

II. EXPERIMENT

We use a large set of (001) $Zn_{1-x}Be_xSe/GaAs$ systems covering the whole composition domain. These were grown by using a Riber 2300 molecular-beam epitaxy system consisting of III-V and II-VI separate growth chambers connected by an ultrahigh-vacuum channel. In a first stage a ~200 nm thick homoepitaxial GaAs buffer layer deposited on a GaAs substrate was grown in the III-V chamber. After this, the samples were transferred to the II-VI chamber. The substrate temperature for II-VI deposition was fixed in the range 300–380 °C, the higher temperatures being used for larger Be contents. The elemental sources were 6N-pure Zn, Be, and Se ingots. The growth rate was typically of 0.5 μm/h. The layer thickness lies in the range 0.7–2.1 μm. Although the layers were not capped, no surface degradation due to contamination or oxidation by atmospheric oxygen was observed, even after months of exposure to air. The composition of the layers was determined from the lattice constant measured by high-resolution x-ray diffraction. A linear dependence of the lattice constant on the alloy composition was assumed (Vegard's law). The large lattice mismatch between the Be- and the Zn-based end compounds of ~9% gives a typical accuracy of ±0.5% in the alloy composition.

Now we summarize briefly the extended characterization of our ZnBeSe samples to figure out their crystalline quality. By using a combination of low-temperature photoluminescence and reflectivity measurements Chauvet, Tournié, and Faurie[20] have evidenced a direct-to-indirect band-gap crossover at the critical Be-content $x_c=0.46$. Below this limit the free exciton recombination line shows up strongly, which indicates high structural quality. However, the photoluminescence linewidth increases smoothly by a factor ~5 from the dilute ($x\sim 0$) to the x_c limit, which suggests progressive degradation of the crystal quality with Be incorporation. The trend is maintained at least up to $x\sim 0.7$, i.e., the highest Be incorporation available at that time, as evidenced by further smearing out of the reflectivity spectra and broadening of the x-ray lines.

Regarding the interfacial quality we notice that lattice matching between the $Zn_{1-x}Be_xSe$ layers and the corresponding III-V buffers should occur at $x\sim 0.03$. Above (below) this limit the epilayers should undergo a tensile (compressive) strain from the substrate, at least at the first stages of the growth. Measurements of the in-plane and out-of-plane lattice constants by high-resolution x-ray diffraction indicate that the ~1 μm-thick layers are fully relaxed from $x\sim 0.25$.[21] Still, reasonable interfacial quality can be evidenced by transmission electron microscopy up to $x\sim 0.5$. Above this limit Raman measurements performed close to the ZnBeSe/GaAs heterojunction with beveled edges obtained by chemical etching indicate that a thin highly disordered layer is deposited before the nominal $Zn_{1-x}Be_xSe$ is grown up to the surface.[22] However, this near-interfacial thin disordered layer was shown to bring negligible signal with respect to the dominant response from the upper thick nominal alloy, whatever the composition.

For each sample unpolarized Raman spectra were recorded by using the conventional and nonstandard backscattering geometries along the [00l]-growth and [l10]-edge crystal axes, respectively. The first geometry (1) is LO allowed and TO forbidden; the situation is reversed in the second geometry (2). The Dilor XY microprobe setup was used since high spatial resolution was needed for geometry 2. By using green excitation, i.e., the 514.5 nm line from an Ar^+ laser, the samples consist in transparent (large gap)/absorbing (small gap) systems so that the spectra recorded with geometry 1 bring the response from both the whole of the layer and the near-interfacial substrate. In some cases this is also true in geometry 2, due to partial overlapping of the ~1 μm in-diameter microprobe on the substrate side. All the spectra were recorded under a standard illumination of 10 MW/cm^2, corresponding to a typical laser output of 50 mW.

III. PERCOLATION MODEL FOR MULTIMODE TO AND LO RAMAN LINE SHAPES

A. Multimode TO and LO Raman line shapes

Recently we have proposed[14] an extension of the Hon and Faust formalism[23] to the equations of motion and polarization given by the MREI model,[2] which is the standard one-bond→one-mode description for the long-wave A-C and B-C phonons in $A_{1-x}B_xC$ zinc blende alloys. Here we use a simplified form obtained by neglecting the second-nearest neighbors in the per-atom force estimate, i.e., by taking the so-called K_{ij} terms in the MREI notation equal to zero. We have checked that this simplification has basically no influence on the final phonon line shapes in our case. Even the simplified form cannot be generalized easily to multioscillator systems, due to the (A,B)-mixed terms. One way is to reformulate via the relative dielectric function ε_r, the $\langle R_A^2\rangle$ and $\langle R_B^2\rangle$ spectral densities, according to the standard MREI notations, which appear in the development of the Raman polarization squared. Labels A and B refer to the A-C and B-C oscillators. We obtain the MREI-like LO cross section with (A,B)-demixed terms:

$$I_{\mathrm{LO}} \propto \mathrm{Im}\left\{ -\frac{1}{\varepsilon_r}\left[1+\sum_p C_p K_p L_p'\right]^2 + \sum_p C_p^2 \frac{K_p^2 L_p'}{4\pi Z_p^2}\right\}. \quad (1)$$

Mintairov *et al.*[24] have obtained a similar expression by considering independent mechanical equations for the A and B oscillators, i.e., not MREI-like, but the present one is *self-consistent* in that all the constituent parameters are x dependent;[2] no additional treatment is needed.

In the basic one-bond→one-mode behavior p=A,B. When the A and/or B single modes split into collections of (A′,A″,…), and/or (B′,B″,…) multimodes, p extends to the relevant number of oscillators. C_p, K_p, L_p' are defined on a per-oscillator basis and refer to the Faust-Henry coefficient of the p mode, to its TO frequency squared, and to the related Lorentzian responses, respectively.[14] Z_p relates to the oscillator strength S_p, and thereby to the $(\mathrm{TO\text{-}LO})_p$ splitting.[2]

S_p and C_p are normalized to the fraction N_p of p oscillators in the alloy with respect to the corresponding parent values. The straightforward relations $\Sigma_A N_A=(1-x)$ and $\Sigma_B N_B=x$ are referred below as the N_p conservation laws.

The LO and TO Raman cross sections are basically extracted from the same set of MREI force equations written on

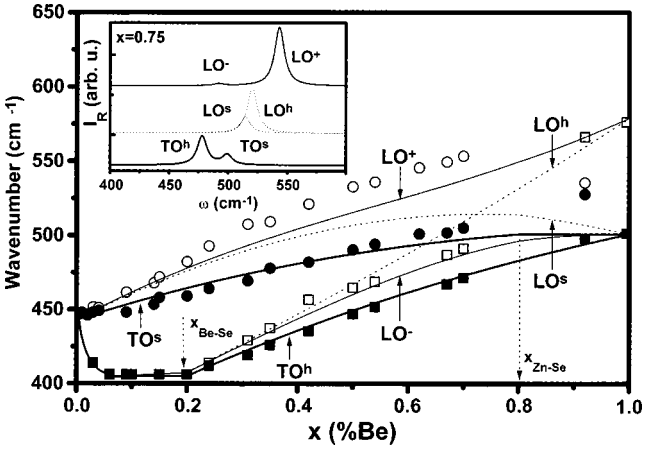

FIG. 1. Two-branches picture for $Zn_{1-x}Be_xSe$ in the Be-Se region. Superscripts *s* and *h* refer to uncoupled Be-Se vibrations within the soft and hard regions, respectively. The thick and thin lines refer to the TO and uncoupled LO modes, respectively. The dotted lines refer to the coupled LO^- and LO^+ modes. The TO (plain symbols) and LO (open symbols) data are shown, for comparison. Examples of the corresponding phonon line shapes close to the anticrossing region is shown in the inset. The LO curves were translated along the vertical axis, for more clarity. I_R and ω are condensed notations for Raman intensity and wave number.

a per-oscillator basis. Only, for the TO mode the Coulomb term related to the ionic character of the bonding is omitted in the force assessment. In Eq. (1) this results in a simplification of the first term, while the second term remains unaffected. It is not necessary to enter the detail since more simplification occurs by considering the Maxwell's equations. Basically the first term in Eq. (1) clearly plays a major role for LO modes, as these correspond to $\varepsilon_r=0$. In contrast it turns negligible for TO modes which correspond to $\varepsilon_r=(qc/\omega)^2$ where q is the magnitude of the phonon wave vector, because $q \gg \sqrt{K_p}/c$ in backscattering geometries. Accordingly for our use I_{TO} reduces to the imaginary part of the second term in Eq. (1).

B. Percolation model for TO modes

Before entering the LO discussion we need a firm TO basis for the stiff Be-Se bond. Our schematic view of a quasisymmetrical double branch with S-shape, only briefly outlined in a previous work,[16] is here directly confronted with the Be-Se data.

The lower and upper $\sqrt{K(x)}$ frequency branches refer to vibrations within the hard Be-rich region and the soft Zn-rich one, respectively. Accordingly in the following the corresponding TO modes and the related parameters are labeled *h* and *s*, respectively. The two branches are fairly described by the thick lines in Fig. 1. Regarding the strength aspect, we have already mentioned that $N_h(x)=x^2$ and $N_s(x)=x(1-x)$.

The lower branch has characteristics very similar to the Be-Te counterpart in ZnBeTe.[16] When x decreases there is first a MREI-like x-dependent portion ($x_{Be\text{-}Se}<x\leqslant 1$) which is referred as the continuum regime, according to the topology of the Be-rich region. At $x\leqslant x_{Be\text{-}Se}$ the fixed TO frequency reveals the fractal nature of the Be-rich bounded clusters. This is referred as the cluster regime. In the Be-dilute limit the branch eventually converges on the frequency of the ZnSe:Be local mode. Detail is given elsewhere.[16] Remarkably the first half of the lower branch ($0<x<0.5$) stays below the TO band, delimited by the ZnSe:Be local mode at $\sim 450\ cm^{-1}$ ($x\sim 0$) and the TO_{BeSe} bulk one at $\sim 500\ cm^{-1}$ ($x\sim 1$). A maximum gap of $\sim 35\ cm^{-1}$ is reached in the fractal regime.

The MREI-like x-dependent portion of the upper Be-Se branch ($0\leqslant x<x_{Zn\text{-}Se}$), which corresponds to the continuum regime for the Zn-rich region, basically fits in the TO band, as would be typically expected in case of a *soft* bond.[16] The same holds true for the Be-Te data.[5] However, careful examination indicates a significant blue departure of the Be-Se data from the curve above $x\sim 0.5$. In particular, from $x=0.67$ the TO^s mode energies are above the bulk TO_{BeSe} mode at $501\ cm^{-1}$. The trend is emphasized in the fractal regime, where the blue shift takes the value of $\sim 30\ cm^{-1}$ from our only sample in this Be range, i.e., $Zn_{0.08}Be_{0.92}Se$. In the Zn-dilute limit the upper branch is expected to converge on the bulk TO_{BeSe} frequency.[16]

In summary the upper and lower Be-Se branches appear to undergo quasisymmetrical excursions out of the TO band in their fractal regime, so that the double branch, tied at the two ends of the TO band, takes a quasisymmetrical overall S shape, schematically.

C. Evidence for LO distortion

By writing that the dielectric function of the alloy turns equal to zero at each frequency ω_p from the whole set of LO multimodes, S_p reformulates as explicit function of the collection of observed $(TO\text{-}LO)_p$ splittings according to

$$S_p=\varepsilon_\infty \frac{(\omega_p^2-K_p)}{K_p}\prod_{m\neq p}\frac{(\omega_m^2-K_p)}{(K_m-K_p)}. \qquad (2)$$

N_p directly follows from the Vegard-like connection between S_p and the corresponding parent oscillator strength.

We have calculated the N_p values via S_p from the observed TO and LO frequencies in our Be-Se spectra. However, the N_p-conservation laws could not be fulfilled, at any alloy composition, in spite of the large flexibility for the location of the overdamped low-frequency LO mode, which typically spreads over more than $100\ cm^{-1}$. The same holds true for the Be-Te data. This is attributed to strong distortion of the Be-VI LO multi mode line shapes, with concomitant impact upon the reliability of the LO frequencies. In the following we investigate the nature of this distortion.

IV. LO SYMMETRY

We show in Fig. 2 the representative TO and LO spectra from the $Zn_{1-x}Be_xSe/GaAs$ system at $x=0.42$. The signal from the GaAs substrate emerges around $280\ cm^{-1}$. In TO symmetry it consists of the narrow TO_{GaAs} mode at $268\ cm^{-1}$. Two broad contributions are observed in LO symmetry. One is a LO-*P* mode located around the TO fre-

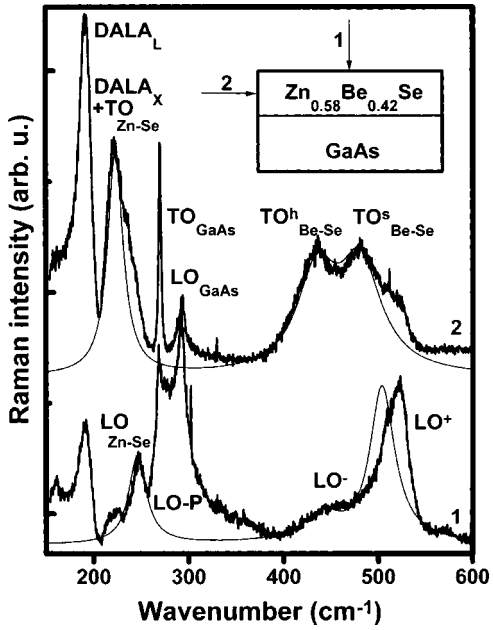

FIG. 2. Raw LO (1) and TO (2) Raman spectra obtained with the $Zn_{1-x}Be_xSe/GaAs$ system corresponding to $x=0.42$ by using backscattering geometries along the [001]-growth and [110]-edge axes, as indicated. The corresponding three-oscillator [Zn-Se, $(Be\text{-}Se)^h$, $(Be\text{-}Se)^s$] curves obtained via Eq. (1) are superimposed after intensity renormalization. The TO curves are translated along the vertical axis, for more clarity.

quency, resulting from coupling between the LO mode and the plasmon excitation (P) in a near-interfacial dense hole gas induced by Zn exposition of GaAs prior to deposition. The other is the uncoupled LO_{GaAs} mode at 292 cm^{-1} from the deep substrate. Extensive detail is given elsewhere.[14]

The Zn-Se domain is located at lower frequency, i.e., $\sim$225 cm^{-1}. Disorder-activated longitudinal acoustical (DALA) bands at the X and L zone edges, referred as $DALA_X$ and $DALA_L$, bring parasitical Raman contributions in this region. This generates a strong Fano interference with the discrete $TO_{Zn\text{-}Se}$ mode, as evidenced by the characteristic antiresonance at $\sim$200 cm^{-1}. The $LO_{Zn\text{-}Se}$ mode, located at higher energy, i.e., $\sim$250 cm^{-1}, is spared.

Mostly on account of the small mass of Be, the Be-Se bonds vibrate at much higher frequency, i.e., in the range 400–600 cm^{-1}. At intermediate x the two Be-Se TO lines have similar intensities, and are quasisymmetrical. In contrast (i) the low-frequency LO mode is weak and overdamped, and (ii) the high-frequency one exhibits a marked red asymmetry. The overall LO line shape remains basically unchanged throughout the whole composition range, while the TO counterpart is extremely x dependent. The same holds true in ZnBeTe.

An additional LO anomaly arises by comparing the experimental TO and LO curves to the corresponding line shapes calculated via Eq. (1) by using a single dielectric function for the three-oscillator system [Zn-Se, $(Be\text{-}Se)^s$, $(Be\text{-}Se)^h$], on the frequency (K_p) and strength (N_p) basis detailed in Sec. III B. The additional parameters needed for the calculations are reported elsewhere.[14]

Good agreement is obtained in the TO symmetry; no adjustable parameter is needed but the linewidth. We have checked that the same holds true throughout the whole composition range, provided the blue departure from the upper branch is taken into account at large x ($x \geqslant 0.5$). Incidentally similar agreement was obtained with our former quantitative approach,[4] where the soft and hard host regions were treated separately. This is because TO modes consist of quasi-independent oscillators. We notice that the agreement is rather poor in the Zn-Se range. This is due to the strong Fano interference between the discrete $TO_{Zn\text{-}Se}$ mode and the DALA continua.

The overall agreement is also good in LO symmetry, but we observe that (iii) the Be-Se high-frequency LO mode emerges at much higher frequency than predicted, which is referred below as the LO blue shift. We have checked that this is true mostly within the percolation range, i.e., the LO blue shift vanishes in the (Be, Zn)-dilute limits. The same behavior is observed in ZnBeTe.

In the following we investigate successively the LO distortions (i)–(iii).

A. LO^- overdamping

Coupling between the individual LO modes from the hard and soft regions via their macroscopic polarization field E becomes allowed by taking a single dielectric function for the hard-soft composite alloy, while this was forbidden with our former approach.[4] E coupling appears to be enough to account for the puzzling overdamping of the low-frequency LO feature at any x (compare the experimental and theoretical LO curves in Fig. 2). Accordingly the low- and high-frequency LO features have a (hard, soft)-mixed character, and thereby cannot be labeled with superscripts h and s, as the TO modes. In the following they are simply referred as LO^- and LO^+, respectively.

Basically E coupling generates a massive $LO^- \rightarrow LO^+$ transfer of oscillator strength. This is responsible for a spectacular increase in the Raman efficiency of LO^+ mode to the detriment of the LO^- mode, which results in quasiextinction of the LO^- mode at any x. Also the LO^- mode is repelled towards the TO^h frequency, while in contrast the LO^+ mode is blue shifted. The full frequency variations versus x of the $TO^{s,h}$ modes (thick lines), the uncoupled $LO^{s,h}$ modes (obtained by using individual dielectric functions, dotted lines), and the coupled LO^- and LO^+ modes (obtained by using a single dielectric function for the whole set of oscillators, thin lines) are displayed in the body of Fig. 1. At low Be content the LO^- mode is h-like while the LO^+ mode is s-like; the situation is reversed at large Be content. A typical coupling-induced anticrossing behavior is observed at $x \sim 0.7$. Detailed insight upon the whole set of phonon lines shapes in this critical x range is shown in the insert of Fig. 1. As a decisive improvement with our former approach[4] the frequency variation versus x of the LO^- mode is explained in a self-consistent way, i.e., no external parameter is needed.

What emerges is that the LO^- overdamping is intrinsic. This rules out former explanation according to which the LO^- overdamping in multiphonon systems would be fortui-

tuous, i.e., the result of a mathematical singularity in the prefactor of the loss term in the LO multimode cross section.[24] One key consequence is that the raw LO frequencies taken from multimode Raman spectra in general are highly unreliable for N_p estimate via Eq. (2), especially close to the anticrossing region, which basically explains the troubles put forward in Sec. III C.

E coupling eventually appears as the key concept for the basic understanding of the one-bond→two-mode percolation behavior in the LO symmetry. This is because the elementary LO modes are necessarily close, which favors strong coupling. Similar *E* coupling was mentioned in the literature, but only between LO modes related to the A-C and B-C bonds in $A_{1-x}B_xC$ alloys.[2,25] This is pertinent when the optical bands from the parent compounds do significantly overlap, which remains rather exceptional. The result is an apparent two-bond→one-mode behavior, currently referred as the mixed-mode behavior. Typical II-VI examples are $ZnSe_{1-x}Te_x$ and $Cd_xZn_{1-x}S$[2]. A recent III-V example is $Ga_{1-x}Al_xN$.[25]

B. LO^+ distortions

Even though the LO^+ experimental line emerges at much higher frequency than predicted, the frequency domains from the experimental and theoretical LO^+ lines do coincide, so that the apparent blue shift of the LO^+ line [distortion (iii)] goes with the marked red asymmetry [distortion (ii)]. Latter naive observation strongly suggests that the distortions (ii) and (iii) have the same origin, corresponding to a recentration of the experimental line towards the upper end of the frequency domain that the LO^+ mode covers. This can be regarded as the result of an intramode "transfer" of oscillator strength, which would basically mirror the $LO^- \rightarrow LO^+$ intermode transfer discussed above.

Actual intramode transfer supposes internal multimode description. The surprisingly large width at half maximum of the BeSe-like TO modes at most *x* values, typically around 30 cm^{-1}, supports latter assumption. The question then is to identify the nature of the predicted multimode behavior.

One possible multimode decomposition *a priori*, which moreover is currently used to account for the LO-related red asymmetries in multinary alloys, is that offered by the much debated[17] spatial correlation model (SCM).[26] Accordingly the overall LO line shape would result from the simple addition of copropagating disorder-induced elementary LO contributions with *q* deviating slightly from the nominal $q \sim 0$ value. However, such approach basically supposes noninterference between long-range LO modes with close frequencies. This view is in contradiction with the existence of coupling effects between polar LO modes, which were shown above to be decisive for the basic understanding of the Be-Se one-bond→two-mode LO behavior. Moreover the SCM fails to account for opposite shift (blue) and asymmetry (red) of a phonon line.

The simplest alternative to SCM is to consider copropagation of *quasi-ideal* $q \sim 0$ elementary modes. In the following we discuss successively the approaches from Brafman and Manor[17] and from Verleur and Barker[18,19] in ternary alloys. Similar multimode descriptions are used for the soft and hard regions, by symmetry.

Our view is that *E* coupling should remain the key concept for the basic understanding of the above one-bond →multimode descriptions in LO symmetry. Indeed, the pioneer's works from Fröhlich,[27–31] related to dipolar waves in biological materials, and Fano,[32] related to plasmon excitations in metals and semiconductors, have shown that the macroscopic longitudinal Coulomb field acts as a carrier of coherence in multiwave polar systems. This key issue, much challenging for the SCM approach in polar alloys, remains unexplored for phonons.

1. LO^+ *blue shift*

Brafman and Manor consider that due to inherent fluctuations in the alloy composition at the atomic scale, LO modes from all alloys $A_{1-x}B_xC$, even those considered as homogeneous at the macroscopic scale, have to be decomposed into collections of $q \sim 0$ elementary modes with slightly different frequencies. Moreover as LO modes currently exhibit asymmetry on the red side, they assume some interaction among the elementary modes which transfers oscillator strength from the less to the more ionic end in the series. This corresponds to the largest TO-LO splitting, and thereby in most cases to the higher-frequency mode. Brafman and Manor clearly pointed out that the polar modes only are concerned with this process, i.e., the LO modes, but the nature of the interaction was unassigned, so that their approach remained qualitative only.

We propose that the transfer of oscillator strength is driven by the macroscopic polarization field that carry the polar LO modes. Accordingly quantitative insight upon the Brafman and Manor's hypothesis can be directly derived by using Eq. (1). For instance we consider the representative *x* value of 0.5 in $Zn_{1-x}Be_xSe$. For a clear overview of the multimode series we start from the TO description, which corresponds to noninteracting elementary modes.

The ultimate description for slight *x* fluctuations is to consider a *continuous x* domain centered on the nominal *x*-value, so that a continuous collection of frequencies is required for proper analysis of the phonon line shape. In our first attempt to mimic frequency continuity, each of the *h* and *s* component is arbitrarily discretized into $n=8$ elementary modes, equally spaced, covering a narrow frequency range of ~ 10 cm^{-1}. A standard width at half maximum of ~ 1 cm^{-1} is typically taken for each elementary mode. This is for the K_p aspect.

As a crude approximation the elementary modes from a given series, i.e., *h* or *s*, are attributed the same starting oscillator strength, although they correspond to different *x* values. Besides a Gaussian-like intensity profile centered on the nominal *x* value is taken, to indicate that the larger the fluctuations in the composition, the more improbable they are. In the end the weighting factors have to fulfill the N_p conservation relations. This is for the N_p aspect. The sharing of the overall BeSe-like oscillator strength and Faust-Henry coefficient among the elementary modes in each series is accordingly derived.

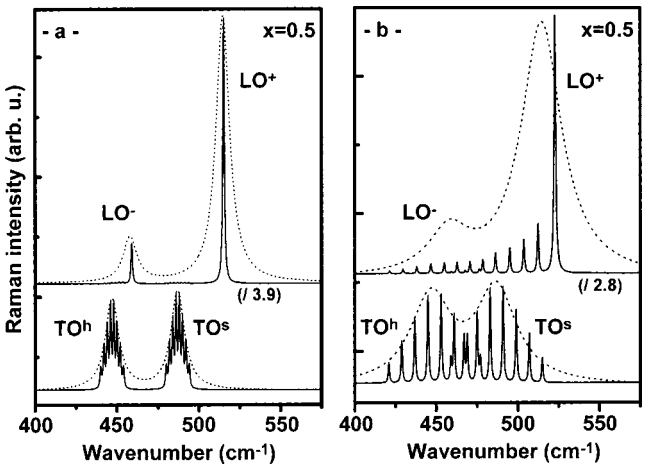

FIG. 3. Be-Se TO (bottom) and LO (top) multimode curves simulated via Eq. (1) in $Zn_{0.5}Be_{0.5}Se$. Eight equally-spaced elementary modes are considered for the *h* and *s* series, with different spacings of 1 cm^{-1} (a) and 3 cm^{-1} (b). The corresponding three-mode [Zn-Se, $(Be\text{-}Se)^h$, $(Be\text{-}Se)^s$] simulations obtained via Eq. (1) are shown (dotted lines), for reference purpose. The LO curves are translated along the vertical axis, for more clarity. The three-more TO curves are superimposed to the multimode ones after proper intensity renormalization. The LO curves can be directly compared to the corresponding TO curves. A normalizing factor, indicated within brackets, must be taken into account for the LO multimode curves.

The resulting TO curve is shown at the bottom of Fig. 3(a). This was obtained after generalization of the standard three-mode [Zn-Se, $(Be\text{-}Se)^h$, $(Be\text{-}Se)^s$] Hon-and-Faust/MREI treatment to the finite collection of $(2n+1)$ oscillators, i.e., after $(2n+1)$ extension of the *p* summation in the TO version of Eq. (1). The multimode and singlemode descriptions are basically equivalent due to noninterference between the elementary modes. The latter simply turns out to be the envelope of the former (refer to the plain and dotted curves) after proper intensity renormalization. The corresponding LO multimode line shape obtained via Eq. (1) is shown at the top of Fig. 3(a) (plain line). The three-mode curve is superimposed (dotted line) after proper intensity renormalization, for comparison.

Basically LO^- and LO^+ intramode transfers of oscillator strength superimpose to the $LO^- \rightarrow LO^+$ intermode transfer, as expected, with the result that the oscillator strength carried by each elementary mode is fully channeled into a single giant oscillation separated from the rest of the series by a blue energy gap. Such condensation in a dense spectrum of polar states is in accordance with the general behavior predicted by Fano.[32] One key point is that the additional intramode transfer eventually generates a LO^+ line slightly blue shifted with respect to the corresponding single-mode prediction. Accordingly multimode decomposition of the *h* and *s* signals is enough to account for the LO^+ blue shift.

2. LO^+ *red asymmetry*

The Brafman and Manor-like description fails to generate the marked red asymmetry of the LO^+ line. We have checked that this does not stay in some technical improvement of the model. In particular, increase in the density of elementary modes for a better approach of continuity in the *s* and *h* series does not modify the $n=8$ picture.

Our view is that the LO^+ red asymmetry indicates partial rather than full intramode transfer of oscillator strength. First partial condensation might arise from screening of the *E* coupling, for some reason. A convenient way to simulate such screening is to introduce by imagination a dense carrier gas in the alloy. The result is to build up a coupled mode between the related plasmon oscillation and the LO multiphonon system. Large plasmon damping is considered, typically holelike, because this is the *sine qua* noncondition to generate a smooth evolution of the LO-*P* frequency from the LO to the TO end references when the carrier density increases, which ideally mirrors progressive screening of the LO-like macroscopic polarization field.[33] Latter behavior actually comes from the simulation (not shown), but there is no intermediary stage of a LO^+ red asymmetry. As a matter of fact a blue asymmetry is rather observed when the LO-*P* mode enters the optical band. In the following the carrier of coherence *E* itself is no more questioned.

The prerequisite condition for effective coupling between two excitations, whatever the nature, is close energy domains. Basically, the closer the energies, the stronger the coupling. Accordingly partial condensation in our multiwaves system may lie in the fact that the *s* and *h* series, consist of *discrete* rather than *continuous* collections of elementary modes. We show in Fig. 3(b) the TO (bottom) and LO (top) multimode line shapes (plain lines) obtained via Eq. (1) by taking $n=8$ equally-spaced elementary modes in the *s* and *h* series, as in Fig. 3(a), but with a spacing enlarged by 3. Due to the reduced mode density the *s* and *h* series eventually turn discrete in character. The three mode TO and LO line shapes are added (dotted lines), for reference purpose. On top of the persistent blue shift of the LO^+ line, which now is very clear, a marked LO^+ red asymmetry eventually shows up, as expected.

With the discrete multimode picture the full set of LO anomalies is eventually accounted for. For a given width at half maximum of the $TO^{h,s}$ modes our simulations indicate that the lower the *n* value, the larger the red asymmetry of the LO^+ line. Therefore *n* is a crucial parameter. One key question is what is the pertinent *n* value to use?

To the best of our knowledge the only discrete multimode description available in the literature is that offered by Verleur and Barker.[18,19] They propose that, at each composition, the entire lattice of $A_{1-x}B_xC$ zincblende alloys is built up from five basic units corresponding to the possible first-neighbor atomic arrangements around the unperturbed C site. If we fix our attention to a single bond, say A-C for instance, Verleur and Barker expect that the strength of this bond, and thereby the frequency of the related vibration, will depend on the other three ions associated with the same C ion. Therefore in a first approximation there are four possible fixed frequencies for the A-C bond in the alloy. Let us label these $\omega_{A\text{-}C}^{(i)}$ where superscript $i=1-4$ refers to the number of A ions at the corners of the C-centered tetrahedrons. A more sophisticated approach is to consider that $\omega_{A\text{-}C}^{(i)}$ is determined not only by *i*, but also by the surrounding tetrahedrons. Thereby

each of the $\omega_{A=C}^{(i)}$ frequency turns x dependent. Besides the proportions f_i of the different units i present in the alloy depend, of course, on the average composition x, and also on a so-called clustering parameter β. This varies from 0 to 1, corresponding to random substitution and maximum amount of clustering of like substituting species around the unperturbed site, respectively. Verleur and Barker provide the $f_i(x,\beta)$ abacuses.[18,19]

Verleur and Barker use the above multimode model in order to explain several subtile spectrally well-distinguishable features in their infrared spectra of partially segregated GaAsP (Ref. 18) and CdSSe (Ref. 19) alloys. Still nothing opposes in principle to its use for the discussion of the Raman spectra from *random* alloys also, which we investigate now. Only, the clustering parameter β has just to be taken equal to zero in this case. Strong experimental support arises by considering that the TO phonon features in the data are unusually broad, even though each of these apparently consists of a single mode. This is not a forbidding character since the envelope of the Verleur and Barker-like multimode TO Raman signal exhibits a single maximum when $\beta=0$, at any x. Examples are given below.

In the following we propose Verleur and Barker-like TO and LO multimode simulations in the random ($\beta=0$) $Zn_{1-x}Be_xSe$ alloys at three representative compositions within the percolation regime, i.e., $x\sim0.25$, ~0.50, and ~0.75. As usual we start from the TO description, for reference purpose.

Direct estimate of the $\omega_{A\text{-}C}^{(i)}(x)$ via *ab initio* calculations is unrealistic at this stage, due to the complexity in the alloy description. As a very crude approximation we take arbitrarily the same constant spacing $\Delta\omega$ between two consecutive elementary TO modes in the *s* and *h* series, and these are centered on the observed $TO^{h,s}$ frequencies. The general MREI trend is that the Be-Se TO modes are blue shifted when x increases. Accordingly the frequencies of the elementary Be-Se TO modes corresponding to $i=1-4$ Be atoms at the corners of the Se-centered units are ranked from the lower to the higher i value in the TO *h* and *s* series, at any x. This is for the frequency (K_p) aspect. Regarding the strength (N_p) aspect, the overall balance between the *h* and *s* series is fixed by $N_h(x)=x^2$ and $N_s(x)=x(1-x)$, as in the three-oscillator [Zn-Se, $(Be\text{-}Se)^s$, $(Be\text{-}Se)^h$] description. The relative strength of the elementary TO modes within each series is then given by $f_i(x,0)$.

The resulting collections of elementary TO modes obtained via the TO version of Eq. (1) are shown at the top of Fig. 4. A very small phonon damping is taken for more clarity. This is larger for the *s* than for the *h* region, to account for the nonideal TO^h/TO^s strength balance at $x=0.5(\neq1)$. The LO multimode line shapes derived via Eq. (1) on the above TO basis are superimposed to the data at the bottom of Fig. 4 (plain line). In each case the three-mode [Zn-Se, $(Be\text{-}Se)^s$, $(Be\text{-}Se)^h$] simulations are added (dotted line) after proper intensity renormalization, for reference purpose. Fair agreement is obtained between the experimental curves and the multimode simulations, in spite of the shortcomings of the model. No adjustable parameter is needed. Basically the LO^- overdamping as well as the blue shift and red asymme-

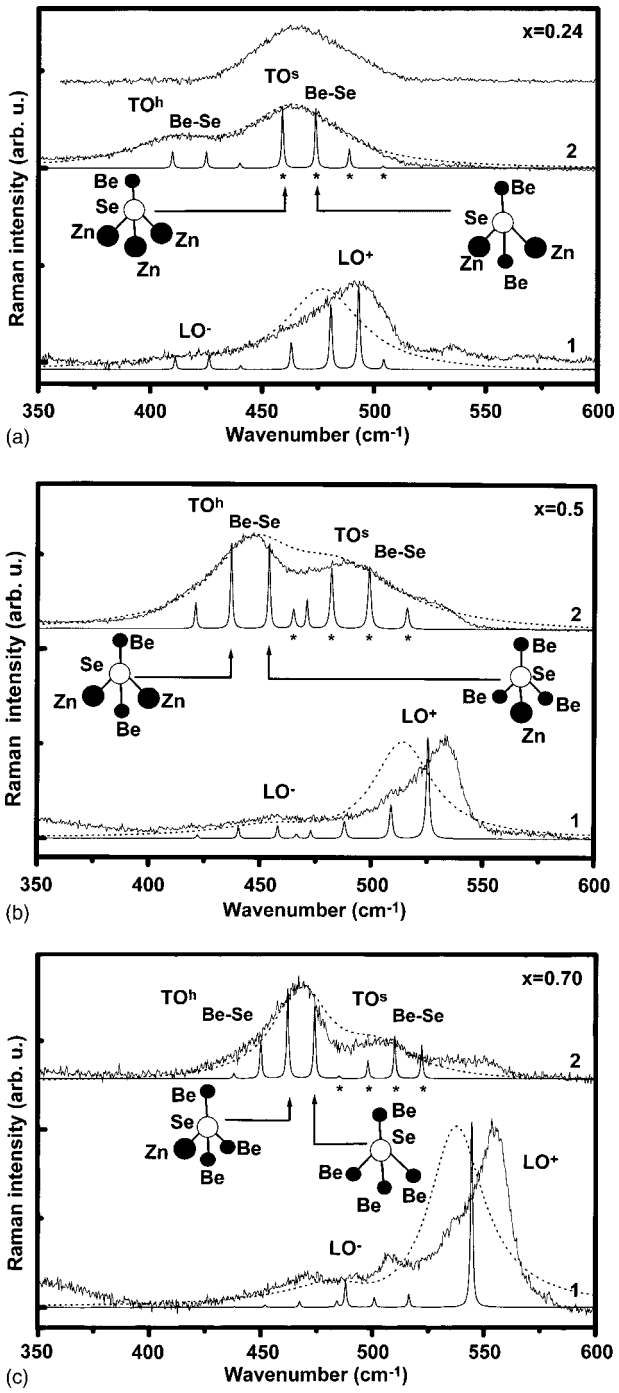

FIG. 4. Raw LO (1) and TO (2) Raman spectra in the Be-Se region of $Zn_{1-x}Be_xSe$ at $x=0.24$ (a), 0.50 (b), and 0.70 (c). The TO curves are translated along the vertical axis, for more clarity. The corresponding Verleur and Barker-like multimode decompositions (thin lines), obtained via Eq. (1), are superimposed after proper intensity renormalization. The starting TO^s series is marked with stars, for more clarity. Each elementary TO mode is assigned the Be-Se vibration within a specific Se-centered tetrahedron unit. The dominant units are schematically indicated. The curves calculated on a three-oscillator [Zn-Se, $(Be\text{-}Se)^h$, $(Be\text{-}Se)^s$] basis (dotted lines) are added, for reference purpose. In part (a) the TO^s mode is cleared from the TO^h contribution for clear insight upon the line shape (top curve).

try of LO^+ the line are simultaneously reproduced.

The units corresponding to $i=1,2$ and $i=3,4$ should be equally dominant at $x\sim 0.25$ and 0.75, respectively. Accordingly the $TO^{s,h}$ modes should exhibit antagonist asymmetries at the two ends of the percolation regime, i.e., bluelike at $x\sim 0.24$ and redlike at $x\sim 0.70$. For clear insight upon the TO profile at $x=0.24$, we clear the dominant *s* line by subtracting the *h* signal, modeled as a symmetrical Lorentzian. The resulting *s* line actually exhibits a blue asymmetry [top spectrum in Fig. 4(a)], as expected. The trend is emphasized when a blue-asymmetrical Lorentzian is taken for contour modeling of the *h* mode. Also, a marked red asymmetry is obvious for the much dominant TO^h mode at $x=0.70$ [top spectrum in Fig. 4(c)].

The antagonist sharing of the oscillator strength between the elementary TO modes at the two ends of the percolation range has decisive impact also on the LO^+ line shape. Basically the transfer of oscillator strength in LO symmetry appears to be all the more efficient that the oscillator strength is carried by the higher-frequency modes in the TO series. Accordingly the linewidth of the LO^+ line reduces when *x* increases, in accordance with the data. The linewidth is as large as $\sim 40\ cm^{-1}$ at $x=0.24$, reduces to $\sim 30\ cm^{-1}$ at $x=0.5$, and falls down to $\sim 20\ cm^{-1}$ at $x=0.70$. The full evolution is given elsewhere.[4] Incidentally alloy disorder and local strain effects are maxima at $x\sim 0.5$, due to the closest intermixing of the hardlike and softlike regions,[4] and thereby fail to explain the above atypical LO behavior.

C. Phonon localization

One key question remains, i.e., why the different local configurations around the Be-Se bonds in the Verleur and Barker units give rise to different Raman peaks, corresponding to as many disorder-induced $q\sim 0$ TO modes? We are not aware that such so-called phonon localization in ternary semiconductor alloys was mentioned before.

According to Anderson's criterion, phonon localization in the Raman spectra is due to disorder-induced $q\sim 0$ frequency fluctuations larger than the $\omega(q)$ dispersion of the related phonon mode.[34] Recent *ab initio* calculations[35] show that the TO modes in bulk BeSe have non-negligible dispersion. Accordingly Be-Se phonon localization would suppose extremely large fluctuations in the Be-Se frequency. This is evidenced in our spectra by the unusually large linewidth of the Be-Se TO lines at significant substitution rate. The problem then is to determine which mechanism is responsible for such large frequency fluctuations.

Our present view is that the mismatch between the Be-Se and Zn-Se bond lengths causes strong local bond distortions. Due to the contrast in the Be-Se and Zn-Se bond-bending force constants, we suggest that the final distortion of a Be-Se bond is strongly dependent on the neighboring bonds and thereby varies much from one Verleur and Barker unit to another, with concomitant impact upon the phonon frequency.

The effect of the Verleur and Barker description in the LO symmetry, i.e., the LO^+ blue shift, is large in the percolation range because, there, the transfer of oscillator strength takes place between several Verleur and Barker units with similar proportion in the alloy. It disappears in the dilute limits because, there, a single Verleur and Barker unit attracts most of the available oscillator strength.

V. CONCLUSION

In this work we enrich our percolation-based picture for the basic understanding of the much puzzling LO Raman line shapes in $Zn_{1-x}Be_xSe$, which opens the class of mixed crystals with contrasted bond stiffness. This is important for future use of this one-bond→two-mode representation in the case of current mixed crystals, i.e., which do not exhibit contrast in the bond stiffness. The study is supported by contour modeling of the TO and LO modes. This is achieved via application of the Hon and Faust treatment to a version of the MREI model generalized to multioscillators. A single dielectric function is used to describe the hard/soft composite crystal.

Coupling between the LO modes via their common longitudinal macroscopic polarization *E* is found to generate numerous puzzling anomalies in the LO symmetry. Two LO components are actually observed, as in the TO symmetry, but these have mixed (hard,soft) character. At low Be content the low-frequency LO^- mode is more hardlike while the high-frequency LO^+ one is more softlike; the situation is reversed at the other end of the composition range, which corresponds to a typical anticrossing behavior at intermediate *x*. Most of all *E* coupling generates a massive $LO^-\rightarrow LO^+$ intermode transfer of oscillator strength. This is responsible for the surprising quasiextinction of the LO^- mode at any *x*. Further understanding of the LO line shapes arises by considering that the contrasts between the Be-Se and Zn-Se bond lengths and bond stiffness force a Verleur and Barker-like discrete multimode response from each region. Accordingly LO^- and LO^+ intramode transfers of oscillator strength superimpose to the $LO^-\rightarrow LO^+$ intermode transfer. This eventually accounts for the blue shift and marked red asymmetry of the LO^+ line. On top of that the multimode description is much helpful for the discussion of both the monotonous decrease of the LO^+ linewidth when *x* increases, and also the subtil antagonism in the asymmetries of the TO line shapes at the two ends of the percolation range.

More generally the puzzling LO behavior can be regarded as the result of a cooperative phenomenon driven by the long-range longitudinal polarization field *E*. This generalizes to discrete assemblies of phonons in mixed crystals the key role of *E* as a carrier of coherence in multiwave polar systems. Also, what emerges is that the Verleur and Barker discrete multimode decomposition provides a much attractive area for the discussion of the asymmetries of the TO and LO Raman line shapes in random alloys in general, which is an issue under current interest, as a possible alternative to the much debated spatial correlation model or to internal/external strain effects.

*Author to whom correspondence should be addressed. Electronic address: pages@ipc.sciences.univ-metz.fr
†Present address: CEM2, Université Montepellier 2-CNRS, 34095 Montpellier, France.

[1] D. W. Taylor, in *Optical Properties of Mixed Crystals*, edited by R. J. Elliott and I. P. Ipatova (North-Holland, Amsterdam, 1988), pp. 35–132.
[2] I. F. Chang and S. S. Mitra, Phys. Rev. **172**, 924 (1968).
[3] D. Stauffer, *Introduction to Percolation Theory* (Taylor and Francis, London, 1985).
[4] O. Pagès, M. Ajjoun, D. Bormann, C. Chauvet, E. Tournié, and J. P. Faurie, Phys. Rev. B **65**, 035213 (2002).
[5] O. Pagès, T. Tite, D. Bormann, O. Maksimov, and M. C. Tamargo, Appl. Phys. Lett. **80**, 3081 (2002).
[6] O. Pagès, T. Tite, D. Bormann, E. Tournié, O. Maksimov, and M. C. Tamargo, Appl. Phys. Lett. **82**, 2808 (2003).
[7] L. Bellaiche, S.-H. Wei, and A. Zunger, Phys. Rev. B **54**, 17 568 (1996).
[8] D. J. Friedman, J. F. Geisz, S. R. Kurtz, and J. M. Olson, J. Cryst. Growth **195**, 409 (1998).
[9] J. Neugebauer and C. G. Van De Walle, Phys. Rev. B **51**, 10 568 (1995).
[10] G. Leibiger, V. Gottschalch, A. Kasic, and M. Schubert, Appl. Phys. Lett. **79**, 3407 (2001).
[11] C. Vérié, in *Semiconductors Heteroepitaxy*, edited by B. Gil and R. L. Aulombard (World Scientific, Singapore, 1995), p. 73.
[12] M. González-Diaz, P. Rodriguez-Hernández, and A. Munoz, Phys. Rev. B **55**, 14 043 (1997).
[13] R. M. Martin, Phys. Rev. B **1**, 4005 (1970).
[14] O. Pagès, M. Ajjoun, D. Bormann, C. Chauvet, E. Tournié, J. P. Faurie, and O. Gorochov, J. Appl. Phys. **91**, 9187 (2002).
[15] O. Pagès, M. Ajjoun, J. P. Laurenti, D. Bormann, C. Chauvet, E. Tournié, and J. P. Faurie, Appl. Phys. Lett. **77**, 519 (2000).
[16] O. Pagès, T. Tite, O. Maksimov, and M. C. Tamargo (unpublished).
[17] O. Brafman, and R. Manor, Phys. Rev. B **51**, 6940 (1995).
[18] H. W. Verleur and A. S. Barker, Phys. Rev. **149**, 715 (1966).
[19] H. W. Verleur and A. S. Barker, Phys. Rev. **155**, 750 (1966).
[20] C. Chauvet, E. Tournié, and J.-P. Faurie, Phys. Rev. B **61**, 5332 (2000).
[21] C. Chauvet, Ph.D. thesis, Centre de Recherche sur 1' Hétéro-Epitaxy est ses Applications (CNRS), Valbonne, France, 2001.
[22] O. Pagès, M. Ajjoun, J. P. Laurenti, D. Bormann, C. Chauvet, E. Tournié, J. P. Faurie, and O. Gorochov, Opt. Mater. (Amsterdam, Neth.) **17**, 323 (2001).
[23] D. T. Hon and W. L. Faust, Appl. Phys. **1**, 241 (1973).
[24] A. M. Mintairov, D. M. Mazurenko, M. A. Sinitsin, and B. S. Yavich, Semiconductors **28**, 866 (1994).
[25] F. Demangeot, J. Groenen, J. Frandon, M. A. Renucci, O. Briot, S. Clur, and R. L. Aulombard, Appl. Phys. Lett. **72**, 2674 (1998).
[26] P. Parayanthal and F. H. Pollak, Phys. Rev. Lett. **52**, 1822 (1984).
[27] H. Fröhlich, in *Cooperative Phenomena*, edited by H. Haken (North-Holland, Amsterdam, 1974), p. 263.
[28] H. Fröhlich, in *Synergetics*, edited by H. Haken (Stuttgart, 1972), p. 241.
[29] H. Fröhlich, Phys. Lett. **39A**, 153 (1972).
[30] H. Fröhlich, Collect. Phenom. **1**, 101 (1973).
[31] H. Fröhlich, in *Coherent Excitations in Biological Systems*, edited by H. Fröhlich and F. Kremer (Springer, Berlin, 1983), p. 1.
[32] U. Fano, Rev. Mod. Phys. **64**, 313 (1992).
[33] J. Geurts, Surf. Sci. Rep. **18**, 1 (1993).
[34] M. Cardona, P. Etchegoin, H. D. Fuchs, and P. Molinàs-Mata, J. Phys.: Condens. Matter **5**, A61 (1993).
[35] G. P. Srivastava, H. M. Tutuncu, and M. Gunhan, Phys. Rev. B **70**, 085206 (2004).